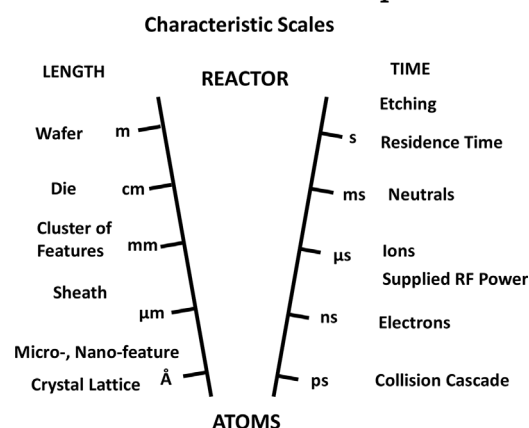


# Hybrid Simulation of Low Temperature Plasmas: A Brief Tutorial

Demetre J. Economou\*

Modeling and simulation of low temperature plasmas is widely accepted as a useful tool from both physics and plasma reactor design points of view. Of the modeling approaches, *hybrid* models strive to combine the predictability of *kinetic* models with the lower computational burden of *fluid* models. This paper presents a brief tutorial of hybrid plasma modeling and representative simulation results using hybrid models. Whenever possible, these results are compared to kinetic and/or fluid simulations as well as experimental data.



## 1. Introduction

Plasma modeling and simulation has emerged as an indispensable activity in low temperature plasma (LTP) science and engineering. It is most impactful when supported by experimental plasma diagnostics. Plasma modeling and simulation can be useful for: (a) unravelling new physics (and chemistry); (b) providing insights into plasma and reactor behavior; (c) explaining experimental data and/or suggesting new experiments; (d) performing “computer experiments” to predict physical quantities that are difficult to measure; (e) providing a platform for the prediction of process outcomes of existing plasma reactors (when, e.g., a new chemistry is employed); and (f) helping in the design of new plasma reactors for etching and deposition processes. See review papers ref.<sup>[1,2]</sup> For an earlier review see ref.<sup>[3]</sup>

One of the main challenges of LTP modeling and simulation is the disparity in length and time scales (Figure 1). Length scales range from atomic (Å, crystal lattice), to microscopic (nm to μm, feature size), to mesoscopic (mm, sheath, cluster of features), to macroscopic (m, reactor, wafer). The range of time scales is also extremely wide, from ps for the collision cascade during ion-surface interaction, to ns response time of electrons (inverse of plasma frequency), to μs response time of ions, to 10–100 ms for heavy species chemistry and gas residence time, to minutes for the duration of etching or deposition processes.

Because of the strong interaction (coupling) of the physicochemical phenomena of LTPs, spanning vast length and time scales, simulation using a “brute force” approach is futile, but also unnecessary. One way to attack the problem is breaking it down into smaller pieces, along naturally occurring length and time scales. For example, a reactor scale simulation can naturally be separated from a feature profile evolution simulation. The former provides boundary conditions (species fluxes, energy, and angular distributions) to the latter. In return, the feature scale simulation generates fluxes of reaction products that enter the reactor simulation (two-way coupling).

Prof. D. J. Economou  
Plasma Processing Laboratory, Department of Chemical and  
Biomolecular Engineering, University of Houston, Houston, Texas  
77204  
E-mail: economou@uh.edu

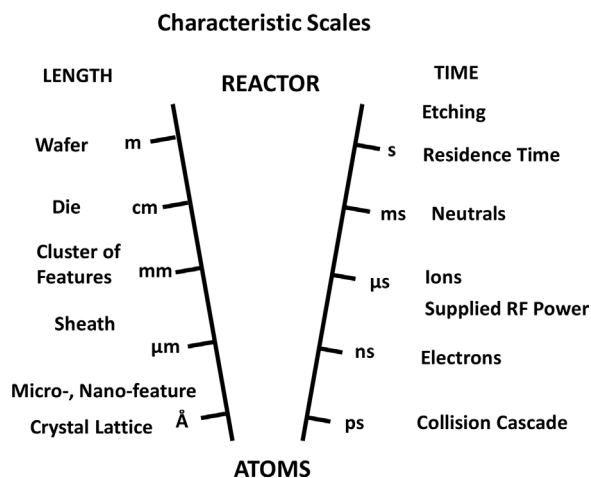


**Figure 1.** Disparity in length and time scales encountered in non-equilibrium plasma modeling and simulation. From atoms to reactor. From ref.<sup>[2]</sup>

To tackle the time scale disparity, the plasma model can be divided into “modules” to separate the time scales of electron, ion, and neutral transport. This is essentially an equation splitting approach. An example of a modular scheme used to simulate an inductively-coupled plasma (ICP) reactor is shown in Figure 2.<sup>[4]</sup> The electromagnetics module (EMM) solves a complex wave equation derived from Maxwell’s equations. Given the coil current, the EMM returns the spatial distribution of power deposited in the plasma. This power is then used in the electron energy module (EEM) to calculate the mean electron energy, or electron temperature for a Maxwellian electron energy distribution function (EEDF). This in turn is used in the neutral transport and reaction module (NTRM) where mass balance equations are solved for the neutral gas species. Reaction rate coefficients of electron-impact reactions are

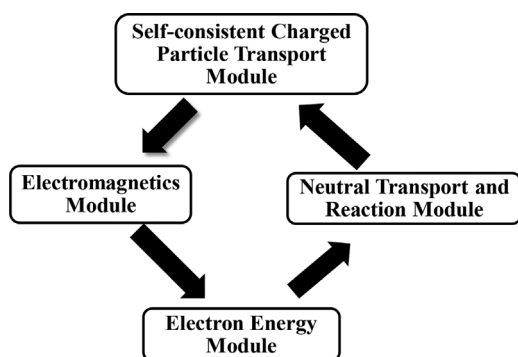


**Figure 2.** Modular approach to tackle the disparity in time scales for modeling an inductively-coupled plasma reactor. This is an equation splitting approach where an equation (or a set of equations) is solved independently in its respective module. Information is cycled between the modules in a hierarchical manner until a converged solution is achieved. From ref.<sup>[4]</sup>

calculated based on the mean electron energy (or  $T_e$ ) obtained from the EEM. The gas composition is fed to the self-consistent charged particle transport module (SCPTM) which solves continuity equations for the mass and momentum of charged species coupled to Poisson’s equation for the electrostatic field. Again, the reaction rate coefficients of electron-impact reactions, as well as electron transport parameters (mobility, diffusivity) required by the SCPTM module, are calculated based on the mean electron energy (or  $T_e$ ) obtained from the EEM. Each of the modules is solved in their natural time scale, for example, ns for the electron energy equation and ms for the neutral transport. The simulation keeps iterating in a hierarchical manner among the modules until convergence has been achieved. It should be remarked that equation splitting in the form of modules does not provide the true time evolution of the system; it only provides the steady-state (or periodic steady-state) result. In order to obtain a time accurate solution (e.g., a pulsed plasma simulation), all model equations must be solved as a group (simultaneously) using the smallest time step required for stability and accuracy.

In this work, a brief tutorial on hybrid simulations of LTPs is presented, with emphasis on capacitively- and inductively-coupled plasma reactors used in the manufacturing of microelectronic devices. This is not intended as an extensive review of hybrid models and simulation results. The paper is organized as follows: An introduction to capacitively- and inductively-coupled plasma reactors is followed by a description of the fundamentals of fluid and kinetic models (including Particle-In-Cell Monte Carlo Collisions, PIC-MCC, and Direct Simulation Monte Carlo, DSMC). Then the most popular hybrid models are discussed and examples of simulation results are given, with emphasis on comparison among the fluid, kinetic and hybrid simulations, and with experimental data. The paper closes with a short summary. It should be remarked that, in addition to LTPs considered here, hybrid simulations have also been applied extensively to problems of magnetically confined fusion and space physics plasmas.<sup>[5,6]</sup>

## 2. Plasma Reactors

The two most common plasma reactors used for microelectronic applications are described below.

### 2.1. Capacitively-Coupled Plasma (CCP) Reactors

Capacitively-coupled plasma (CCP) reactors have been (and continue to be) a workhorse in microelectronic device fabrication. CCP tools are widely employed in etching and deposition applications because they can provide uniform

processing and better control of feedstock gas “cracking” by the plasma. Figure 3 shows a schematic of a parallel plate CCP reactor. One of the electrodes is connected to a radio frequency (RF, usually 13.56 MHz) power supply through a blocking capacitor (more generally an impedance matching network, not shown), while the counter-electrode is grounded. The substrate electrode can be made large enough to hold many wafers, but single wafer tools (processing one wafer at a time) are almost exclusively used for improved process control. Figure 3 shows a symmetric configuration (electrodes of equal area), that is normally operated at relatively high pressures (>100 mTorr); this is the so-called plasma etching configuration. As a result of collisions in the sheath, the energy of ions bombarding the wafer is rather low (<100 eV), and the ion angular distribution is wide. In asymmetric systems (different electrode areas), the sheath over the smaller electrode attains a larger voltage resulting in a (negative) DC bias. Conditions of high (in absolute value) DC bias and low pressure (1–10 s of mTorr) can yield intense ion bombardment of the wafer. This is referred to as *reactive ion etching* (RIE) or reactive sputter etching. A disadvantage of the CCP reactor is that the plasma (electron and ion) density can not be controlled independently of the ion bombardment energy. As the applied RF voltage amplitude is increased to increase the plasma density, so does the sheath potential and consequently the ion bombardment energy. Excessive ion energy is not beneficial as it can lead to unwanted sputtering and heating of the wafer. Dual-frequency (or multi-frequency) CCPs have been developed to partially achieve independent control of the flux and energy of ions bombarding the substrate.<sup>[7]</sup> For example, power at relatively high frequency (e.g., 10–100 MHz) is used to control plasma production (hence ion density and flux), while power at relatively low frequency (e.g., 1–10 MHz) is used to control ion energy. Another way to control the ion energy (and the ion energy distribution) is to apply tailored voltage waveforms.<sup>[8]</sup>

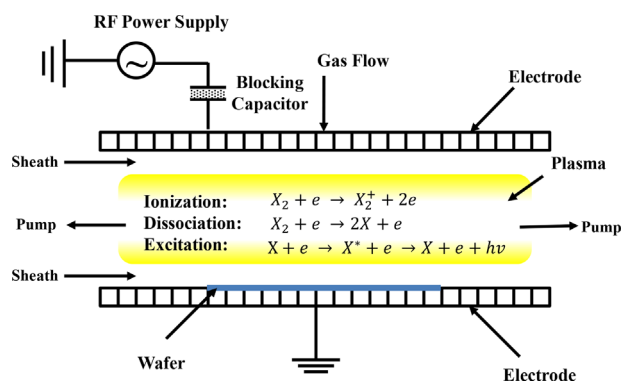
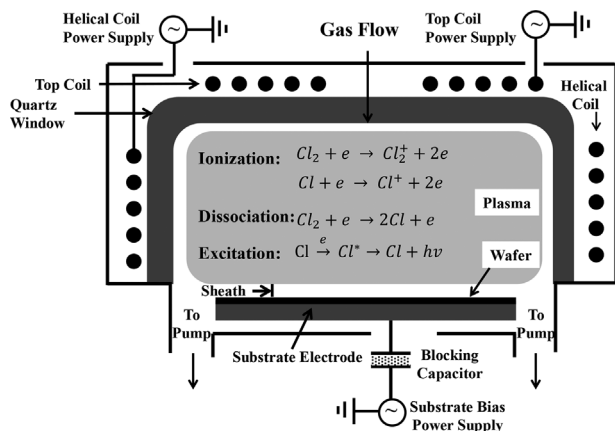


Figure 3. Schematic of a parallel plate capacitively-coupled plasma (CCP) reactor.

The electron heating mechanism in CCPs depends on pressure. At low pressures (typically <10 mTorr), stochastic heating by the oscillating sheaths dominates, while at higher pressures (>100 mTorr), ohmic heating takes over.<sup>[9]</sup> The EEDF is typically Druyvesteyn-like at higher pressures but it turns into bi-Maxwellian at low pressures.<sup>[10]</sup> The bi-Maxwellian is composed of a population of cold electrons that reside in the bulk plasma, and can not reach the sheath to be heated, due to the existence of the ambipolar potential well, and a population of hot electrons that can overcome the bulk potential barrier and reach the sheath where they are heated. At high enough plasma densities, electron–electron collisions make the EEDF approach a Maxwellian. This typically happens when the degree of ionization of the gas  $n_e/N \gg 10^{-4}$ , where  $n_e$  is the electron density and  $N$  is the neutral gas density.

## 2.2. Inductively-Coupled Plasma (ICP) Reactors

Etching of nanoscale structures requires extreme directionality of the impinging ions. This can only be achieved by avoiding ion collisions in the sheath. Furthermore, etching of wafers with ever increasing diameter demands a uniform plasma over large areas (300–450 mm diameter). In an effort to satisfy these requirements, high (charge) density, low (gas) pressure plasmas were developed.<sup>[11]</sup> Salient features of these so-called high density plasma (HDP) reactors are: (a) (quasi) independent control of plasma density and ion bombardment energy can be achieved by substantially decoupling plasma generation from substrate (wafer) bias; (b) high plasma density (i.e., small Debye length, implying thin sheath) and low gas pressure (long mean free path) result in a collisionless sheath that promotes ion directionality; and (c) low gas pressure facilitates species diffusion, promoting uniformity over large diameter substrates. Examples of HDP are ICP, helical resonator, electron cyclotron resonance (ECR), and helicon sources.<sup>[12]</sup> ICPs are particularly attractive because their design is relatively simpler and they are scalable to large diameter substrates.<sup>[13,14]</sup> In ICPs, the plasma is excited in a cylindrical chamber ( $r, z, \theta$ ) by a helical (solenoidal) or planar (stovetop-type) coil powered at radio frequencies, most often at 13.56 MHz (Figure 4). The coil current generates a time-varying magnetic field (mainly in the  $z$ -direction along the coil axis), which in turn induces an azimuthal (in the  $\theta$ -direction) electric field that couples power to the plasma, that is, heats the electrons. For common excitation frequencies (less than the electron plasma frequency), the electromagnetic fields are absorbed by the plasma within the *skin depth*. For typical conditions, fields penetrate a few centimeter into the plasma. The power is deposited non-uniformly in the shape of a toroid. Because of the low pressure, however, species diffusion is facile and the plasma fills the whole reactor. In the absence



**Figure 4.** Schematic of a dual coil inductively-coupled plasma (ICP) reactor.

of any capacitive coupling from the coil, the plasma is quiescent with a relatively low plasma potential ( $\sim$ few  $T_e$  or  $\sim$ 15–20 V) thus minimizing unwanted sputtering of the reactor walls. Capacitive coupling from the coil can result in larger and oscillating plasma potential. The electrode holding the wafer can be biased independently by a separate RF power supply in order to control the energy of ions bombarding the wafer. As in the case of capacitive coupling from the coil, larger (but controllable) time-dependent plasma potentials are then established.

### 3. Plasma Modeling and Simulation

There are two primary models used for plasma simulation, namely, fluid and kinetic. The basic principles as well as advantages and disadvantages of each of these models are briefly outlined below. Hybrid models are derived by combining fluid and kinetic models.

#### 3.1. Fluid Models

Fluid models are generally applicable when the Knudsen number,  $Kn = \lambda/L < 0.1$ . Here,  $\lambda$  is the species mean free path (mfp), and  $L$  is a characteristic length scale of the reactor (e.g., interelectrode spacing). To account for highly non-equilibrium situations (sharp gradients), one can set

$$L = \varphi / \left| \frac{\partial \varphi}{\partial x} \right| \quad (1)$$

where  $\varphi$  is, for example, number density or temperature. One can think of situations where the fluid approximation is valid in parts of a reactor, but not in others. For example, the length scale of the bulk plasma may be large enough for  $Kn < 0.1$  to be satisfied, but that may not be the case in the sheath, which sustains sharp gradients (small  $L$ ).

In a fluid simulation one solves continuity equations for species density, momentum, and energy. These are derived as *moments* of the Boltzmann equation.<sup>[15]</sup> To achieve “closure” of the continuity equations, however, an assumption must be made regarding the species velocity distribution function. The most common assumption is that of a Maxwellian distribution.

The main advantage of fluid simulations is a speedy calculation relative to the corresponding kinetic simulations. This allows more complex chemistries to be included, and parametric investigations to be conducted to ascertain the effect of reactor design and operating parameters on discharge characteristics and process outcomes (e.g., rate, uniformity, etc.). The main disadvantage of fluid simulations is that only “average” values of the dependent variables are obtained, instead of the corresponding distribution functions.

The fluid model equations include:

(a) the species number density continuity Equation (2) (where  $i$  can be electrons, positive ions, negative ions, or neutrals),

$$\frac{\partial n_i}{\partial t} + \nabla \cdot (n_i \mathbf{u}_i) = \sum_j R_{ij} \quad (2)$$

where  $n_i$  and  $\mathbf{u}_i$  are the density and average velocity of species  $i$ , respectively.  $R_{ij}$  is the rate of production or loss of species  $i$  due to the volumetric reaction  $j$ ,

(b) the (vector) momentum equation,

$$\begin{aligned} \frac{\partial}{\partial t} (n_i m_i \mathbf{u}_i) + \nabla \cdot (n_i m_i \mathbf{u}_i \mathbf{u}_i) \\ = -\nabla P_i + n_i q_i \mathbf{E} - n_i m_i \mathbf{u}_i \nu_{mi}, \end{aligned} \quad (3)$$

where  $\nu_{mi}$  is an effective momentum-exchange collision frequency of species  $i$  and  $P_i$  is its partial pressure given by  $P_i = n_i k T_i$ , where  $T_i$  is the temperature,  $q_i$  is the charge, and  $k$  is Boltzmann’s constant. Equation (3) assumes that the pressure tensor is isotropic which appears to be a good approximation in the absence of strong magnetic fields. In Equation (3), the terms represent (in order from left to right) local acceleration, convective acceleration, motion due to pressure gradient, motion due to force fields (e.g., electric field), and momentum exchange due to collisions with the background species. When the terms on the left hand side of Equation (3) are negligible (see ref.<sup>[15]</sup> for a discussion of this point), one obtains,

$$\mathbf{J}_i = \pm \mu_i n_i \mathbf{E} - D_i \nabla n_i \quad (4)$$

where  $\mathbf{J}_i = n_i \mathbf{u}_i$ , and  $\mu_i$  and  $D_i$  are the species mobility and diffusivity, respectively. Equation (4) assumes isothermal medium and neglects the flux due to convective neutral flow. The (+) and (–) signs correspond to positive ions and

electrons or negative ions, respectively. Equation (4) is known as the drift-diffusion approximation (DDA) and is often used in place of the full momentum Equation (3).<sup>[16–18]</sup> The DDA has been questioned at low pressures and in the sheath, where species inertia (left hand side of Equation (3)) may not be negligible.<sup>[19]</sup> Under typical conditions, the drift flux dominates over the diffusion flux in Equation (4) for positive ions, while the two fluxes nearly balance each other (and are in opposite direction) for electrons and negative ions. This balance results in the Boltzmann relation, which for electrons reads (with  $T_e$  in  $V$ ),

$$n_e = n_{e0} \exp(-V/T_e) \quad (5)$$

where  $n_{e0}$  is the electron density at the point where  $V=0$ . Although electrons are mobile enough (due to their small mass) to respond to the variations of the applied electric field (i.e., the electron inertia may be neglected), ions are massive and may not be able to follow the field faithfully. Recognizing this fact, Richards et al.<sup>[20]</sup> introduced an equation for an “effective” field to which the ions respond.

$$\frac{\partial \mathbf{E}_i^{eff}}{\partial t} = \nu_{mi}(\mathbf{E} - \mathbf{E}_i^{eff}) \quad (6)$$

That way, the drift-diffusion Equation (4) can be used for both electrons and ions, except that the actual electric field is replaced by the effective field, in the case of ions. Of course, when the full momentum Equation (3) is used, Equation (4) and (6) become immaterial.

(c) the equation for the average electron energy  $\bar{e}$  is written as,

$$\begin{aligned} \frac{\partial}{\partial t}(n_e \bar{e}) + \nabla \cdot \left[ \frac{5}{3} \mu_e n_e \mathbf{E} \bar{e} - \frac{5}{3} D_e \nabla(n_e \bar{e}) \right] \\ + e \mathbf{J}_e \cdot \mathbf{E} + 3 \nu_{me} \frac{m_e}{M} n_e k(T_e - T_g) \\ + \sum_j R_{ej} H_{ej} = 0 \end{aligned} \quad (7)$$

here,  $H_{ej}$  is the loss (or gain) of electron energy due to collision  $j$ . In order from left to right, the terms in Equation (7) represent the time rate of change of the energy density ( $n_e \bar{e}$ ) of electrons, convective transport of energy, energy transport by conduction, work done on the electrons by the electric field (ohmic heating), electron energy loss in elastic collisions, and electron energy loss in inelastic collisions (or gain in superelastic collisions). In RF plasma systems, in addition to ohmic (Joule) heating, non-ohmic heating is also important, especially at low pressures ( $<10$  s mTorr).<sup>[21,22]</sup> The ability of the fluid model to capture this non-ohmic heating has been scrutinized.<sup>[23]</sup> Turner<sup>[24]</sup> proposed a modification to the fluid equations to account for non-ohmic heating.

(d) finally, the Poisson equation links the potential field to the charge density,

$$\epsilon_0 \nabla^2 V = - \sum_i q_i n_i \quad (8)$$

here  $\epsilon_0$  is the vacuum permittivity,  $V$  is the electrostatic potential, and  $q_i$  is the charge of species  $i$ . Depending on the approximations made, different sets of the equations shown above are used by different authors. Most often, the drift-diffusion approximation is made for both electrons and ions.<sup>[25–27]</sup> Other authors solve the full momentum equations for either electrons or ions (using drift-diffusion for the other species)<sup>[28]</sup> or for both electrons and ions.<sup>[29,30]</sup> An energy equation for ions is normally not solved. Almost always, it is assumed that ions are at the same “temperature” as neutrals, because of the effective energy exchange between ions and neutrals, having comparable masses. At very low pressures (or more accurately for high  $Kn$ ) this is not a good assumption. Most workers assume a neutral gas temperature  $T_g$ . Others solve an energy balance for the neutral gas to calculate  $T_g$ .<sup>[31]</sup>

Typical boundary conditions are given in ref.<sup>[32–34]</sup> Boundary conditions for the mass continuity Equation (2) specify a zero electron density at the wall, or an electron flux equal to the local thermal flux multiplied by an electron absorption coefficient. This boundary condition can also include a flux of secondary electrons produced by, for example, ion bombardment of the wall. The positive ion diffusion flux is set to vanish at the wall, that is, ion transport is dominated by drift at the wall. The negative ion density is set to zero at the wall since negative ions are confined by the electrostatic potential of the plasma (but not in an ion–ion plasma!). The neutral species boundary condition is set such that the flux is equal to the reaction rate at the wall. The latter is often specified through a “sticking” or reaction probability. Care should be exercised to account for rarefaction effects at low pressures; see Chantry for a discussion.<sup>[35]</sup> An “extrapolation” boundary condition (second derivative of velocity equal to zero) is typically specified for the momentum Equation (3).<sup>[29]</sup> Boundary conditions for the electron energy equation have included a constant energy (or temperature) at the wall, or adiabatic wall. More often, the energy flux is set equal to the electron number flux multiplied by the energy carried by each electron to the wall ( $2T_e$  for Maxwellian EEDF). Boundary conditions on the Poisson Equation (8) include a specified potential on metal surfaces (e.g., grounded or RF driven) or a specified current at a metal wall. The potential at the surface of a dielectric is calculated using Gauss’s law:

$$(\mathbf{D}_2 - \mathbf{D}_1) \cdot \mathbf{n} = \sigma_s \quad (9)$$

$$\frac{d\sigma_s}{dt} = J_e \bullet \mathbf{n} + J_i \bullet \mathbf{n} \quad (10)$$

where  $\mathbf{D}_1$  and  $\mathbf{D}_2$  are the electric displacement vectors,  $\sigma_s$  is the net charge density accumulated on the dielectric surface, and  $\mathbf{n}$  is the surface normal unit vector pointing outwards. Only the normal components of the electron current density and total ion current density contribute to surface charging, Equation (10).

### 3.2. Kinetic Models

Kinetic models yield the particle (ion, electron, neutral) distribution functions as an output of the simulation. The electron energy distribution is used to calculate the electron transport properties (mobility, diffusivity) and electron-impact reaction rate coefficients. The ion energy distribution on the substrate governs the etching rate, while the ion angular distribution controls etching anisotropy. Averaging over the distribution function yields the number density, velocity, and average energy of the species. Kinetic simulations are considered more accurate than fluid simulations, especially at low pressures, when the Knudsen number,  $Kn = \lambda/L > 0.1$ . Kinetic simulations, however, are computationally expensive when compared to fluid simulations. Kinetic simulations include Particle-In-Cell with Monte Carlo Collisions (PIC-MCC),<sup>[36–39]</sup> Direct Simulation Monte Carlo (DSMC),<sup>[40–43]</sup> and direct solution of the Boltzmann equation.<sup>[44,45]</sup>

#### 3.2.1. PIC-MCC Simulation

The plasma particle kinetics can be described by the Boltzmann Equation (11) in the 7-dimensional co-ordinates of phase space ( $\mathbf{x}$ ,  $\mathbf{v}$ ), and time,  $t$ .

$$\frac{\partial f}{\partial t} + \mathbf{v} \bullet \frac{\partial f}{\partial \mathbf{x}} + \frac{\mathbf{F}}{m} \bullet \frac{\partial f}{\partial \mathbf{v}} = \left( \frac{\partial f}{\partial t} \right)_{coll} \quad (11)$$

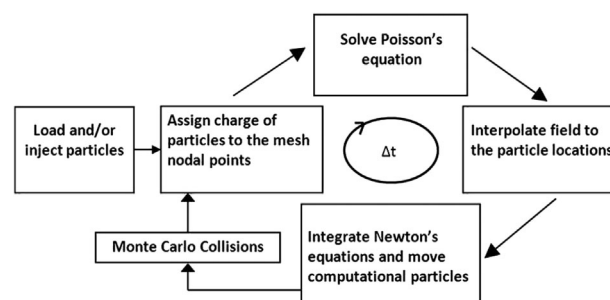
here  $\mathbf{x}$  and  $\mathbf{v}$  are particle (vector) location and velocity, respectively, and  $f$  is the particle distribution function. The right hand side of Equation (11) is the collision operator.  $\mathbf{F} = q(\mathbf{E} + \mathbf{v} \times \mathbf{B})$  is the Lorentz force acting on a particle with charge  $q$ . The Lorentz force is found by solving Maxwell's equations for the electric field  $\mathbf{E}$  and magnetic induction  $\mathbf{B}$ .

The PIC-MCC simulation<sup>[36–39]</sup> essentially solves the Boltzmann Equation (11). The most common case reported in the literature so far is  $1d3v$ , that is, simulation in one spatial dimension but with all three velocity components of the particles accounted for in collisions. The sequence of operations to complete a single loop of a PIC-MCC simulation is shown in Figure 5. A mesh (grid) is overlaying all the computational particles (or superparticles). The mesh cell size  $\Delta x$  must be smaller than the smallest

physical dimension that needs to be resolved (e.g., the Debye length if electrons are solved using PIC). Superparticles move according to Newton's equation of motion,

$$\begin{aligned} \frac{d\mathbf{x}}{dt} &= \mathbf{v} \\ \frac{d\mathbf{v}}{dt} &= \frac{\mathbf{F}}{m} \end{aligned} \quad (12)$$

the time step  $\Delta t$  of an explicit integration of Equations (12) must obey the Courant condition,  $(v\Delta t/\Delta x) < 1$ , where  $v$  is the particle speed. The next step is collisions among the particles. Most commonly, collisions are handled by Monte Carlo using the null-collision technique.<sup>[46]</sup> The minimum collision set includes elastic, excitation and ionization collisions of electrons with the gas. Elastic and charge exchange (CX) collisions of ions with background neutrals are also included. Of particular importance are symmetric CX collisions due to their large cross section. In charge exchange, an ion transfers its charge to a neutral with negligible momentum exchange. If the ion happens to be energetic (e.g., CX occurs in the sheath), the result of the collision will be a high energy directional neutral and a low energy (thermalized) ion. In symmetric CX collisions a daughter ion interacts with its parent neutral. Returning to Figure 5, after the Monte Carlo collision step, the charge of each particle is distributed to the nodal points of the computational mesh using, typically, bilinear interpolation (weighting). Based on the resulting charge density, Poisson's equation is solved and the electric field is calculated at the nodal points. The electric field is then interpolated at the location of the particles using again a bilinear function (another weighting). The new electric field gives a new Lorentz force on the particles for the next motion time step. The cycle is repeated until steady-state (or periodic steady state) is reached. For typical CCP or ICP reactors this takes  $\sim 1000$ s of RF cycles. The simulation predicts the flux, as well as the energy and angular distributions of electrons, and ions as a function of position including the electrode surface where the substrate rests.



■ Figure 5. Flow chart of PIC-MCC simulation procedure.

### 3.2.2. Direct Simulation Monte Carlo (DSMC)

DSMC<sup>[40–43]</sup> was first developed for the simulation of rarefied gas flows, such as those found in aerodynamics. DSMC solves the Boltzmann Equation (11) in the binary collision approximation. The flow domain is divided in a number of cells. The cell size is determined by the *local* mean free path  $\lambda$ ; a size  $\sim \lambda/3$  is typically recommended. The flow field is simulated using a number of particles (simulated molecules or superparticles); some  $10^7$  superparticles are not atypical for runs on multi-node clusters. The type, spatial coordinates, velocity components, internal energy, and weight factor of each superparticle are stored in the computer. The weight factor is the number of real molecules represented by each superparticle. The statistical fluctuations of DSMC solutions are inversely proportional to the square root of the total number of superparticles ( $N$ ). The computational burden is proportional to  $N$ . As the superparticles move through the reactor, they collide with one-another and with the walls of the reactor. Feed gases may be introduced at specified inlet port locations, and superparticles may be removed from the simulation because of chemical reactions (in which case their identity changes) or through the pumping port(s). The basic premise of DSMC is that the motion of simulated molecules can be decoupled from their collisions over a time step. The size of the time step is selected to be a small fraction of the mean collision time,  $\Delta t = \lambda\pi/(2 \bar{u})$ , where  $\bar{u}$  is the most probable speed,

$$\bar{u} = \sqrt{(2kT_0)/M} \quad (13)$$

$T_0$  being a reference temperature. During the motion phase, simulated molecules move in free flight according to Newton's law (deterministically, see Equation (12)), given their starting velocity and the forces acting on them (e.g., electric field force on ionized species). During this phase, superparticles may cross cell boundaries, collide with walls, or exit the flow field. During the collision phase, collision pairs are selected from within each cell regardless of the position of the superparticles within the cell. It is imperative that the collision frequency occurring in the actual flow field is simulated correctly. The no-time-counter (NTC) method<sup>[41]</sup> is most frequently used to handle collisions. The cross section as a function of energy for all collision types must be known. The hard sphere or the variable hard sphere collision models are most commonly used.

## 4. Hybrid Models and Simulations

Hybrid models have been developed<sup>[47–49]</sup> in an attempt to preserve the accuracy and wealth of information of kinetic

models, and at the same time reduce the computational burden. Some common hybrid modeling approaches are discussed below.

### 4.1. Fluid-EEDF Hybrid

The most common hybrid, namely Fluid-EEDF hybrid, is a fluid description of the discharge, except that the electron transport properties and electron impact reaction rate coefficients are obtained from a calculation of the electron energy distribution function (EEDF). The latter is found by solving the Boltzmann Equation (11), either directly<sup>[44,45]</sup> or via a Monte Carlo scheme.<sup>[48,49]</sup> The fluid “module” can include the species mass, momentum, and energy continuity equations, and Poisson's equation for the electric field. No equation is necessary for the (mean) electron energy, since the EEDF is sought as part of the solution. Solution of the Boltzmann equation (in, say, the EEDF module) requires as input the space and time variations of the electric field. This is provided by the fluid simulation. The fluid simulation also provides the ion flux bombarding the electrode that may produce secondary electrons. If needed to account for electron-electron collisions in the EEDF module, the fluid module can also provide the electron density. The overall simulation alternates between the fluid module and the EEDF module until convergence.

A variant of this hybrid is encountered when a beam of high energy electrons pierces through the discharge.<sup>[50]</sup> A typical case is emission of secondary electrons due to ion, electron, or photon bombardment of the electrode (or substrate). Such electrons accelerate in the sheath electric field and gain energy up to the maximum sheath potential, before entering the bulk plasma. Because of their high speed, beam electrons (sometimes called runaway electrons) do not collide frequently in the gas phase (electron impact collision cross sections usually drop off at high energies), and they can reach the surface of the opposite electrode with considerable energy. When they do collide, during their crossing of the interelectrode gap, beam electrons produce excitation and ionization of the gas. In this variant of the Fluid-EEDF hybrid, the beam electrons are treated by a Monte Carlo simulation to calculate their EEDF. The low energy electrons are treated as fluid, including an energy balance for low energy electrons in the fluid module. The dividing line between low and high energy electrons for an argon plasma, for example, is the threshold of the first excitation of argon atoms. In some cases, fluid equations for the beam electron density and average energy are used. The model then becomes an all fluid model.

Monte Carlo simulations of multidimensional EEDFs can be time-consuming. Spatial averaging of the distribution function under the so-called *non-local approximation* (NLA) can offer great simplification.<sup>[47,51–53]</sup> In the NLA, the

multidimensional Boltzmann equation can be turned into an ordinary differential equation in total (kinetic plus potential) energy, that is, a 1-D equation. This simplification is applicable provided that the electron energy relaxation length  $\lambda_e$  is larger than the plasma reactor dimension,  $L$ .

$$\lambda_e = \lambda \sqrt{\frac{M}{m_e}} > L \text{ or } \lambda_e = \sqrt{\lambda \lambda^*} > L \quad (14)$$

The left (right) equation gives the electron energy relaxation length for elastic (inelastic) collisions, respectively. Here,  $\lambda^*$  is the mean free path for inelastic collisions. However, for the operating conditions of practical reactors, the NLA may not be applicable to the whole range of electron energies. Specifically,  $\lambda_e > L$  may be valid for the energy range of elastic collisions, but not for the inelastic energy range. Recognizing this fact, Kortshagen and Heil<sup>[54]</sup> developed a model of a 2-D ICP based on a hybrid approach. They used the NLA for electrons with kinetic energy below the threshold energy for excitation of the working gas (argon in this case), and the spatially dependent ( $r, z$ ) Boltzmann equation for higher energy electrons. The ions were described as fluid while the solution of the complex wave equation provided the azimuthal RF electric field that heated electrons. Instead of solving the Poisson equation, electroneutrality was assumed. Not having to solve Poisson's equation reduces the computational burden tremendously since the dielectric relaxation time ( $\sim 1$  ps) that limits the time step in explicit solutions of the Poisson equation is eliminated. Of course, only the bulk plasma can be assumed electrically neutral. The sheath has to be spliced to the bulk plasma solution. Simulated plasma density and potential profiles<sup>[54]</sup> agreed with Langmuir probe measurements. In addition, the simulation could capture the transition from on- to off-axis peak ionization as pressure was increased (a non-local effect), also in agreement with experimental data. More recently, Loffhagen and Sigeneger<sup>[45]</sup> focused attention on hybrid models that combine a fluid description of the plasma with the Boltzmann equation for a kinetic description of electrons. They employed the two-term approximation, assuming that the anisotropic part of the distribution responds fully to the time variations of the field (quasi steady-state approximation). A direct solution of the Boltzmann equation, neglecting electron-electron collisions, was employed by Matsui et al. in their relaxation continuum-Boltzmann equation model.<sup>[55]</sup>

A comprehensive hybrid model, HPEM or hybrid plasma equipment model, is described by Kushner (see review article ref.<sup>[56]</sup>). HPEM consists of a hierarchy of modules, each solving for a physical process in disparate timescales. One can mix and match different modules depending on the perceived physics. Figure 6 shows, a comparison of the 2-D electron density and (equivalent) electron temperature

profiles predicted by HPEM for an argon ICP at 10 mTorr, and 300 W inductive power at 10 MHz.<sup>[56]</sup> The substrate was biased with an independent power supply with a sinusoidal waveform of 200 V amplitude at 5 MHz. The difference between the two panels is the way the electrons were handled. In Figure 6 (top), an equation for the average electron energy was used in what can be considered to be an all fluid model. In Figure 6 (bottom), a Monte Carlo simulation (including electron–electron collisions) was used to determine the EEDF, in what can be considered to be a hybrid model. In addition, the hybrid model included non-local power deposition (anomalous skin effect) by calculating the plasma currents with the MC simulation and passing them back to an electromagnetics model maintaining a self-consistent simulation. The fluid and hybrid models predict similar density profiles (Figure 6). This is not surprising since, at steady-state low pressure plasmas, the charge density often assumes the fundamental diffusion mode. The absolute value of the density is overestimated by the fluid model by a factor of 2. The difference is not severe considering the very different physics captured by the different models. The electron temperature profiles predicted by the fluid and hybrid models are different. In particular,  $T_e$  peaks directly under the coil in the fluid model, and decreases monotonically away from that region. The temperature gradient is quite small implying large thermal conductivity of the electron gas, due to the high electron density. In the hybrid model,  $T_e$  again peaks under the coil but it also has a local minimum on axis. This may be due to entrapment of low energy electrons by the ambipolar electric field in the bulk plasma. These electrons are not energetic enough to climb the potential barrier and penetrate into the skin layer to be heated.

A comprehensive 2-D ( $r, z$ ) hybrid model of a DC glow discharge in argon (used for spectrochemical analysis) was developed by Bogaerts.<sup>[57]</sup> She used a combination of fluid, Monte Carlo and collisional-radiative models to predict the species densities (including excited states and hyperthermal or fast atoms), electric field distribution, energy distribution of electrons, ions and fact neutrals, and ultimately the depth profile of the crater formed in the copper cathode as a result of sputtering of the cathode.

The Fluid-EEDF hybrid is not to be confused with fluid simulations that use *offline* solutions of the Boltzmann equation (using, e.g., BOLSIG+ ref.<sup>[58]</sup>) to calculate the electron transport and electron-impact reaction rate coefficients as a function of E/N or average electron energy,  $\bar{\epsilon}$ . To save computation time, look up tables are prepared a-priori that provide the electron transport and reaction parameters as a function of E/N or  $\bar{\epsilon}$  for different gas compositions. Interpolation is used to extract these parameters for use in the fluid model. Two cases can be distinguished under this category: (a) Use of the local field



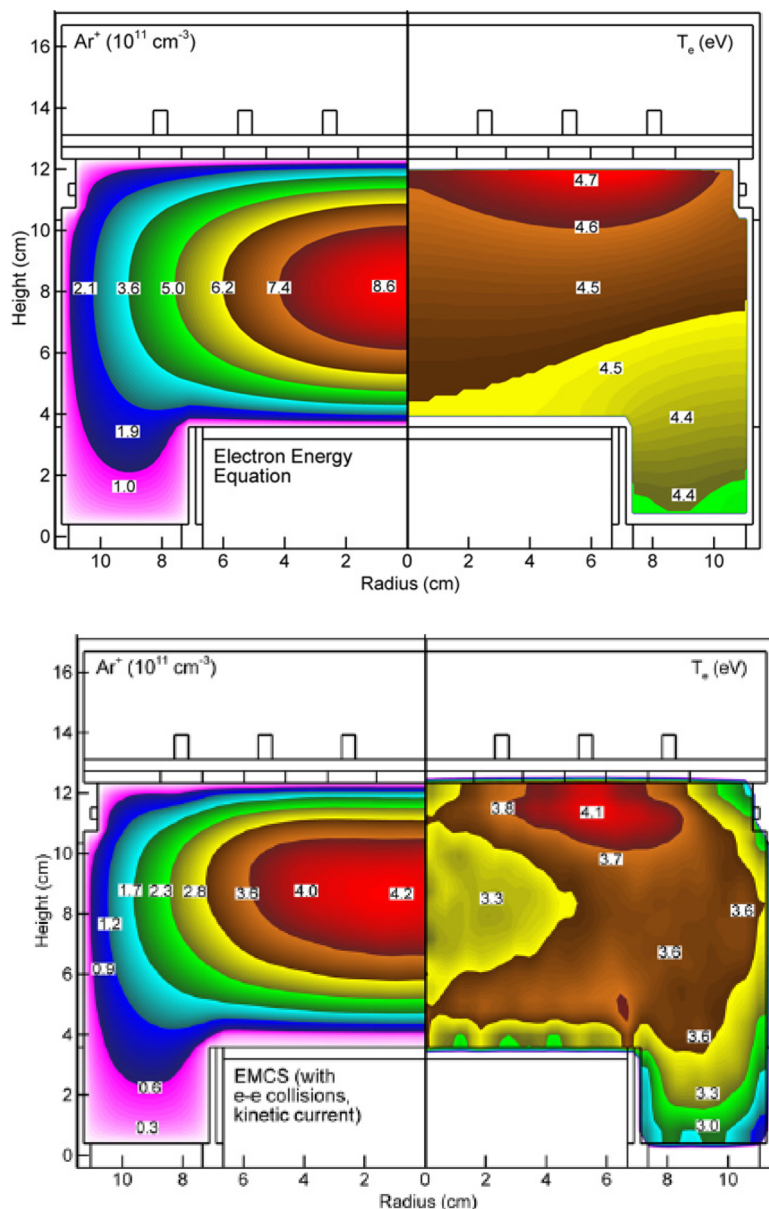


**Figure 6.** Ion density and effective electron temperature profiles in an argon ICP at 10 mTorr, 300 W inductive power, and 200 V peak bias at 5 MHz on the substrate. The model used was the same for both figures except for the treatment of electrons: (top) an electron energy equation was used in a fluid model, (bottom) the EEDF was found using Monte Carlo simulation (including electron–electron collisions), and current in the plasma was non-local (i.e., not based on Ohm’s law). From ref.<sup>[56]</sup>

approximation (LFA). Under this approximation the electron (and ion) transport and reaction parameters depend on the value of the local electric field. The LFA implies that the collision frequency is high enough for the distribution function to reach quickly the state that would be obtained under a constant DC electric field of value equal to that in the RF discharge at the location of the electron. In this case, an electron energy balance is not

necessary. The electric field is calculated using the Poisson Equation (7). The LFA may be applicable in atmospheric pressure, LTPs owing to the high collisionality at high pressure. However, the LFA can not capture non-local effects. (b) Use of an equation for the average electron energy  $\bar{\epsilon}$  or effective electron temperature, defined as  $T_{eff} = 2\bar{\epsilon}/3$ . A fluid model that includes an equation for  $\bar{\epsilon}$  can partially capture non-local effects.

Hwang et al.<sup>[59]</sup> compared the results of a fluid model of a CCP with those of a PIC-MCC model and a fluid-EEDF hybrid. The hybrid used a Monte Carlo simulation of the EEDF producing electron transport and reaction coefficients for the fluid model. They used the drift-diffusion approximation (Equation 4) instead of the full momentum Equation (3). Figure 7 shows, a comparison of the plasma densities predicted by the fluid, PIC-MCC, and hybrid simulations as a function of pressure. For each pressure, both the ion (solid lines) and electron (dashed lines) densities are shown. The hybrid simulation predicts results similar to those of the PIC-MCC simulation (even on a quantitative comparison) except for the transition from 50 to 100 mTorr. This turned out to be a transition between the  $\alpha$  and  $\gamma$  modes of the discharge. The fluid simulation predicts a plasma density within a factor of 2 compared to the kinetic (and hybrid) simulation. The fluid simulation predicted the opposite trends of electron temperature (calculated as 2/3 of the average energy) versus pressure at the center, when compared to the PIC and hybrid simulations (not shown). Such “temperature” comparisons, however, are complicated because of the different shape of the EEDF (e.g., Druyvesteyn vs. bi-Maxwellian) as pressure decreases.

Fluid models can be one- (1-D), two- (2-D), or three-dimensional (3-D). Zero dimensional (0-D) or “global” models<sup>[11]</sup> can be considered limiting cases of fluid models where there are no spatial gradients. In these models, surface processes (e.g., wall recombination of radicals) are converted to volumetric terms by multiplying by the surface-to-volume ratio. Analytical (or semi-analytical) models are used to relate the value of ion density in the bulk to that at the sheath edge. For example, positive ion losses to the wall are expressed in terms of the product of Bohm velocity and density of ions at the sheath edge. An  $h$ -factor is used to relate the densities of the ions in the well-mixed bulk and the sheath edge.<sup>[11]</sup> Global models

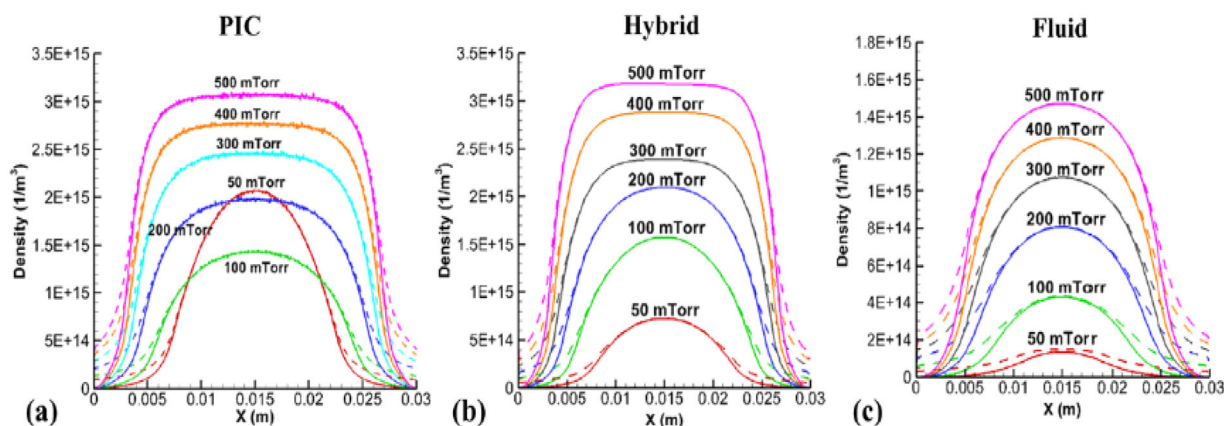


**Figure 7.** Comparison among PIC-MCC, hybrid, and fluid simulations of plasma density profiles in an argon ICP for different gas pressures. For each pressure, both the ion (solid lines) and electron (dashed lines) densities are shown. From ref.<sup>[59]</sup>

may be useful for sorting out the chemistry in complex gas plasmas. Because of the very short computation times (typically of the order of seconds), comprehensive chemical reaction networks with a multitude of species may be included in the model. Sensitivity analysis<sup>[60]</sup> may provide a reduced reaction set that may be used in a spatially resolved simulation of the system. Hybrid models using a global model for the plasma coupled with a kinetic model for the EEDF are a special case of Fluid-EEDF hybrids. An example of such a hybrid is given in ref.<sup>[61]</sup> This hybrid combines a kinetic simulation for electrons (so-called Dynamic Monte Carlo simulation) with a global model of the bulk plasma and a collisionless sheath to describe high-density low-pressure ICP reactors.

#### 4.2. DSMC-Fluid Hybrid

DSMC-Fluid (DSMC-F) hybrid models treat ions and neutrals as particles (kinetically) and electrons as fluid. The reason for treating ions and neutrals kinetically is that these are the species involved in reactions on the wafer surface. The DSMC-F hybrid simulation provides the fluxes and energy and angular distributions of ions and neutrals bombarding the wafer. These are critical for simulating the shape evolution of microfeatures during etching or deposition. The simplest treatment of electrons is to model them as fluid in which the electric field force balances the pressure force in the simplified form of the momentum balance Equation (4). The electric field is then,

$$E = -\frac{\nabla(n_e k T_e)}{en_e} \quad (15)$$

this equation becomes the Boltzmann relation (Equation 5) by further assuming isothermal plasma ( $T_e = \text{const.}$ ) The electric field of Equation (15) is used to move ions in the

DSMC simulation. Using this approach, Gatsonis and Yin<sup>[62]</sup> simulated the plume emanating from a pulsed plasma thruster. They used a combination of DSMC and PIC to model neutrals and ions. A fluid model was used for electrons. Electroneutrality was assumed and the electric field was obtained using ambipolar charge flow. Simulation results showed the existence of backflow of both ions and neutrals. Shimada et al.<sup>[63]</sup> used DSMC for neutrals and ions along with fluid electrons to study neutral depletion in low pressure Ar/N<sub>2</sub> discharges. They observed severe neutral depletion due to gas heating and also due to the electron pressure becoming a significant fraction of the total pressure thus lowering the pressure of the neutral gas. In another DSMC-Fluid hybrid approach, the electron properties and the electric field were calculated based on a self-consistent all fluid model of a chlorine ICP reactor. The model included Poisson's equation in the whole domain resolving the (very thin) sheath.<sup>[42]</sup>

Figure 8 shows, the 2-D profiles of the radial component of the gas velocity (left panel) and the neutral gas temperature (right panel) in the reactor. The velocity is highest at the gas injection port. The velocity at the upper parts of the cylindrical chamber is in part due to ion neutralization on the wall, and reflection of the resulting neutrals back into the plasma. The radial velocity crosses zero around the horizontal central plane of the reactor. The gas temperature shows a maximum in the reactor center. Gas heating is a result of ion-neutral collisions (especially charge exchange), creation of hot neutrals due to molecular chlorine dissociation (Frank-Condon effect) and to a lesser degree electron-neutral collisions.

#### 4.3. PIC-MCC-Fluid Hybrid

In classical PIC-MCC simulations, ions and electrons are treated as particles (see section 3.2.1) in a cold, uniform

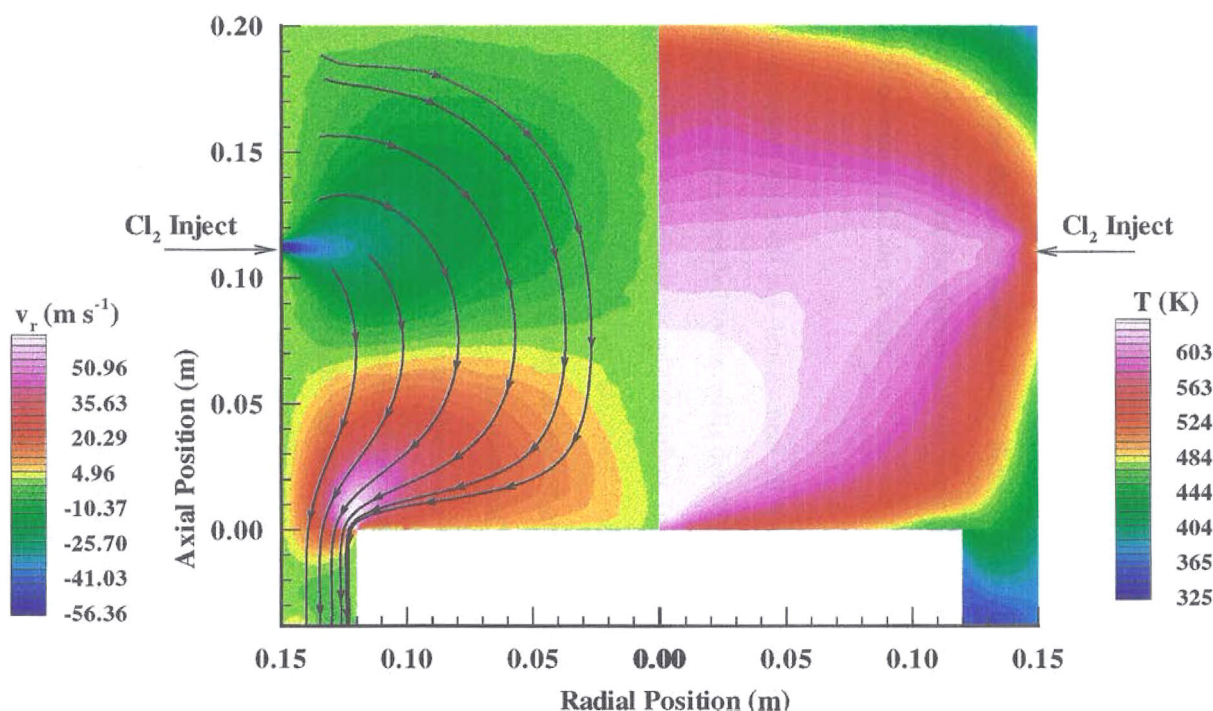


Figure 8. DSMC-Fluid hybrid simulation of a chlorine ICP. (left) Radial component of fluid velocity; representative streamlines are also shown. (right) Gas temperature distribution in the reactor. From ref.<sup>[42]</sup>

density background neutral fluid. The simplest PIC-MCC-Fluid hybrid treats the ions as particles moving in the ambipolar field established by a quasi-neutral isothermal electron fluid. Solution of the Poisson equation is not necessary in this case; electroneutrality is assumed, instead. Clearly this is applicable to the bulk plasma only and not the sheath. A more common PIC-MCC-Fluid hybrid treats ions as particles and electrons as fluid obeying the Boltzmann relation.<sup>[64,65]</sup> This approximation speeds up the simulation significantly, since phenomena on the time scale of electrons (e.g., plasma oscillations) are not resolved. Thus, the cell size  $\Delta x$  can be larger than the Debye length and the time step  $\Delta t$  can be larger than the inverse of the electron plasma frequency. Kwok<sup>[66]</sup> assumed a bi-Maxwellian EEDF and used two Boltzmann relations, one for the hot and another for the cold electron populations. Poisson's equation was solved in this case, so the sheath was naturally accounted for.

Furthermore, in classical PIC-MCC simulations, neutral species transport and reaction are not considered, due to the disparity in time scales of electron, ion, and neutral dynamics. The feedstock gas is assumed to be a motionless background medium with uniform density. For practical systems where reactor design is in focus, this assumption may be problematic, especially in high density plasmas, where severe gas heating causes substantial neutral density gradients. In addition, important etching or

deposition radicals produced by dissociation of the gas, as well as excited states (e.g., metastables) are not taken into account.

Diomede et al.<sup>[67]</sup> presented a one-dimensional in space, three-dimensional in velocity ( $1d3v$ ) hybrid model which couples a Particle-in-Cell model with Monte Carlo Collisions (PIC-MCC) for charged species, with a reaction-diffusion fluid model for neutrals. In the case of  $H_2$  discharge, five charged species (electrons,  $H^+$ ,  $H_2^+$ ,  $H_3^+$ , and  $H^-$  ions) and 15 neutrals (14 vibrational levels of the electronic ground state of  $H_2$ , and  $H$  atoms) were accounted for. The density of neutral species  $n_c$  was obtained by solving the 1-D reaction-diffusion equation, neglecting fluid flow. This implies that the Peclet number  $Pe = uL/D$  is very low (diffusive transport):

$$\frac{\partial n_c(x, t)}{\partial t} - D_c \frac{\partial^2 n_c(x, t)}{\partial x^2} = \sum_r (v'_{rc} - v_{rc}) k_r \prod_q n_q^{v_{rq}} \quad (16)$$

where  $D_c$  is the diffusion coefficient of species  $c$ , and  $v_{rc}$  is the stoichiometric coefficient of the  $c$ -th species in the  $r$ -th elementary reaction. Primed ( $v'_{rc}$ ) and un-primed ( $v_{rc}$ ) stoichiometric coefficients refer to reaction products and reactants, respectively. For electron impact reactions, the corresponding rate coefficient  $k_r$  was calculated through the electron distribution  $f_e$ , as found from the PIC-MCC model,

$$k_r(x, t) = \sqrt{\frac{2}{m_e}} \int_0^{\infty} \varepsilon f_e(\varepsilon, x, t) \sigma_r(\varepsilon) d\varepsilon \quad (17)$$

where  $\sigma_r(\varepsilon)$  is the reaction cross section as a function of electron energy  $\varepsilon$ . Wall reactions included in the fluid model were deactivation of vibrationally excited molecules (reaction probability  $\gamma_V$ ) and recombination of H atoms (reaction probability  $\gamma_H$ ).

The energy distributions of positive ions bombarding the electrode, predicted by this PIC-MCC-Fluid hybrid, are shown in Figure 9. The  $H_3^+$  IED (Figure 9a) shows the classical bimodal structure,<sup>[68]</sup> centered around the average sheath potential (127 V), and a tail towards lower energies due to ion-neutral collisions. The bimodal structure results by ions entering the sheath in different phases of the RF cycle, experiencing a different accelerating potential, depending on when they entered the sheath. The predicted bimodal distribution, with a more intense peak at lower energy, is close to the experimental IED obtained under similar conditions,<sup>[69]</sup> reproduced here as Figure 9b. The ion transit time through the sheath can be estimated by  $\tau_i \approx 2\bar{s}/\sqrt{2e\bar{V}_s/m_i}$ , where  $\bar{s}$  and  $\bar{V}$  are the time-average sheath thickness and sheath potential, respectively, and  $m_i$  is the ion mass.<sup>[68]</sup> This yields an ion transit time of 405 and 331 ns, respectively for  $H_3^+$  and  $H_2^+$ , while the RF period is  $\tau_{RF} = 73.75$  ns. Therefore, the ratio  $\tau_i/\tau_{RF}$  is 5.5 and 4.5, respectively for  $H_3^+$  and  $H_2^+$ . The smaller the  $\tau_i/\tau_{RF}$  ratio, the wider the IED. The most structured IED is that of  $H_2^+$  ions (Figure 9c), which exhibits multiple peaks. These peaks can be explained by symmetric charge exchange collisions. If such a collision takes place in the sheath, the newly created ion will experience only a fraction of the sheath voltage. The collision is symmetric and has a large cross section if it involves the parent gas and the daughter ion. The computed  $H_2^+$  IED is in good agreement with the experimental results,<sup>[69]</sup> reproduced here as Figure 9d. The IED of  $H_3^+$  does not have extra peaks, because these ions can not suffer symmetric charge exchange collisions, and the cross section for asymmetric charge exchange is much lower.

Eremin et al.<sup>[70]</sup> proposed a PIC-Fluid hybrid for highly collisional RF helium discharges between parallel plate electrodes. Electrons were treated by PIC-MCC while heavy species were treated as fluid. The ion momentum equation was either the drift-diffusion approximation (DDA), or the full momentum balance (including inertia). The dependence of the ion mobility on the electric field was taken into account. Figure 10 shows, a comparison of the plasma density profiles predicted by PIC-MCC and two versions of the hybrid simulation; HC1 refers to the hybrid simulation that uses the full ion momentum balance Equation (3). HC2 refers to the hybrid simulation where the ion momentum is described by the drift-diffusion approximation with field dependent mobility (variant of Equation (4)). Figure 10 shows that the hybrid

simulation accounting for ion inertia is in excellent agreement with PIC-MCC, while the hybrid simulation using the DDA overestimates the peak electron density by about a factor of 2.

Surendra<sup>[71]</sup> employed a well-defined system to perform a benchmark comparison of a CCP simulation including fluid, PIC-MCC, and hybrid models. Simulation results were provided by 12 research groups from the US and Europe. A 1-D He RF discharge was simulated using identical cross sections or swarm parameters, under specified conditions of interelectrode spacing, pressure, applied current density, etc. There was good agreement in the results (plasma density, ionization rate, ion flux on electrode, etc.) among the PIC-MCC simulations, and also between PIC-MCC and hybrid simulations. Fluid simulations showed greater variation in their prediction of some discharge parameters (RF voltage, plasma density), but not in others (ion flux on electrode). In general, the differences were exacerbated at lower pressure (30 mTorr). Interestingly, some of the fluid simulations were in good agreement with the PIC-MCC and hybrid simulations, even at low pressure where the fluid simulations were expected to deviate considerably from the kinetic (and hybrid) simulation predictions.

#### 4.4. Non-Local Effects

When electrons are warm enough to be transported out of the “skin layer” of an ICP during an RF cycle, power is said to be deposited non-locally. In a sense, the current at a given location is influenced by the electric field at all other locations. In contrast, in the local case, the current at a given location only depends on the field at that particular point (Ohm’s law). Non-locality is typically characterized by the parameter  $l/\delta_0$ , where  $l = \bar{u}_e/\sqrt{\omega^2 + \nu^2}$  is an “effective” electron mean free path, and  $\delta_0$  is the classical skin depth,

$$\delta_0 = \frac{c}{\omega_p} \left(1 + \frac{\nu^2}{\omega^2}\right)^{1/4} \quad (18)$$

Here  $\bar{u}_e = \sqrt{2eT_e/m_e}$  is the most probable electron speed,  $\omega_p$  is the electron plasma frequency ( $\omega_p = \sqrt{e^2 n_e/\varepsilon_0 m_e}$ ),  $\omega$  is the applied RF frequency,  $c$  is the speed of light in vacuum,  $\nu$  is the electron momentum-transfer collision frequency,  $T_e$  is the electron temperature, or effective electron temperature (in V), and  $m_e$  is the electron mass. When  $(l/\delta_0)^2 \gg 1$ , non-local behavior dominates. The reason is that when the effective mfp of electrons is much longer than the skin depth, electrons gain energy in the skin layer, and exit that layer (thus keeping their energy) before the RF field reverses. These energetic electrons deposit their energy through collisions in locations away from the skin layer (non-locally).

Ramamurthi et al.<sup>[72]</sup> developed a self-consistent hybrid (fluid-kinetic) model to study the effect of non-local electron

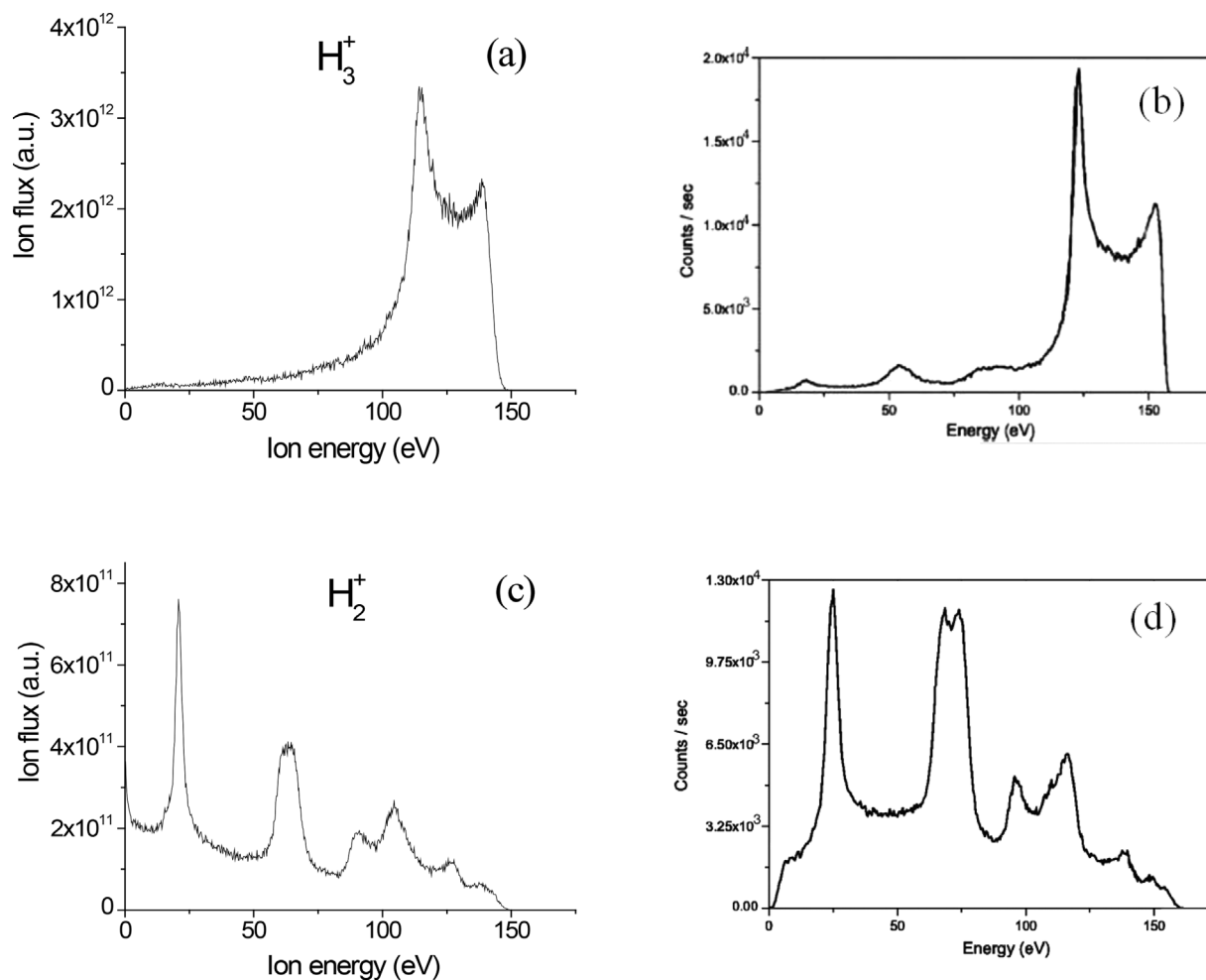


Figure 9. (a) Ion energy distribution (IED) of  $H_3^+$  calculated using a PIC-MCC-Fluid hybrid model. (b) Measured  $H_3^+$  IED. (c) IED of  $H_2^+$  calculated using a PIC-MCC-Fluid hybrid model. (d) Measured  $H_2^+$  IED. From ref.<sup>[67]</sup>

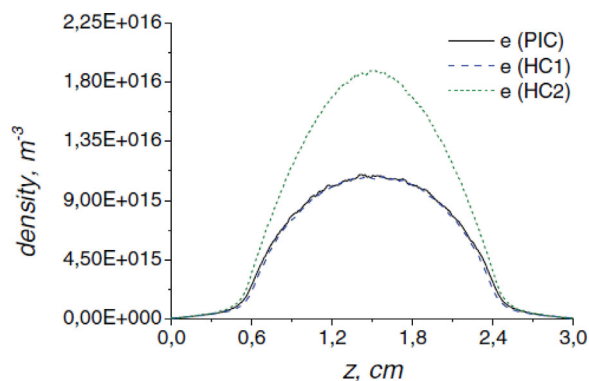
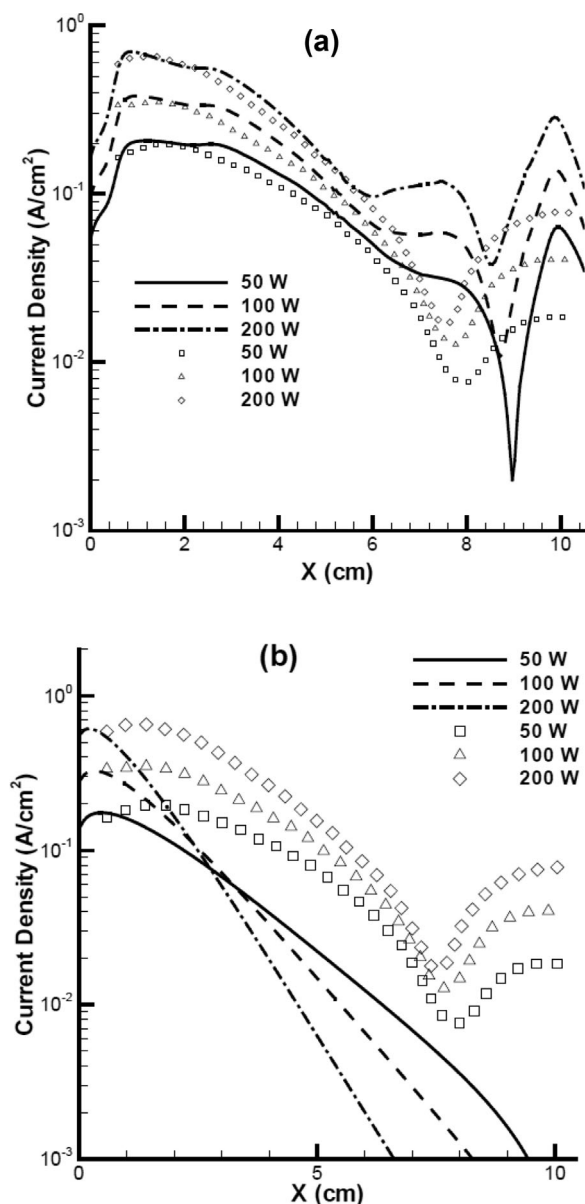


Figure 10. Helium ion density profiles in a parallel plate atmospheric pressure plasma reactor predicted by PIC-MCC (solid line), hybrid 1 (dashed line), and hybrid 2 (dotted line). See text for HC1, HC2. From ref.<sup>[70]</sup>

conductivity on power absorption and plasma density profiles in a planar inductively coupled discharge at low pressures ( $\leq 10$  mTorr). The model consisted of three modules: (a) an electron energy distribution function (EEDF) module to compute the non-Maxwellian EEDF; (b) a non-local electron kinetics module to predict the non-local electron conductivity, RF current, electric field, and power deposition profiles in the non-uniform plasma; and (c) a heavy species transport fluid module to solve for the ion density and velocity profiles as well as the metastable density. Results using the non-local electron conductivity model were compared with predictions of a local theory (Ohm's law), under otherwise identical conditions. The RF current, electric field, and power deposition profiles were very different, especially at 1 mTorr for which the effective electron mean free path was larger than the skin depth. Figure 11 shows, a comparison of RF current density versus position as predicted by the simulation and measured experimentally<sup>[73]</sup> at a pressure of



**Figure 11.** Spatial profiles of current density in an argon ICP at 1 mTorr and different powers, predicted by a hybrid model (lines), compared to experimental data (points): (a) simulation used a non-local conductivity model; and (b) simulation used a local (Ohm's law) conductivity model. From ref.<sup>[72]</sup>

1 mTorr. When the non-local conductivity formulation is used in the hybrid model, the current goes through local minima and maxima in the plasma body. Such non-monotonic behavior is the signature of non-local electron transport. In this case, the agreement between simulation predictions and measurements is reasonable. However, when the local conductivity (Ohm's law) is used with the hybrid model, the predicted RF current is essentially monotonic and it is grossly underestimated compared

to the measurements. Nevertheless, the plasma density profiles (not shown) were almost identical (within 10%) for the same *total* power deposition in the plasma. This result suggests that, for the purpose of computing plasma densities, a local conductivity model (Ohm's law), with much reduced computational expense, may be employed even in the non-local regime.

## 5. Summary

Modeling and simulation of LTPs is widely accepted as a useful tool from both the physics and plasma reactor design points of view. There are two primary models applied to plasmas: fluid and kinetic. The main advantage of fluid models is the relatively speedy calculation, compared to kinetic models. This allows more complex chemistries to be included, and parametric investigations to be conducted to ascertain the effect of reactor design and operating parameters on discharge characteristics and process outcomes (e.g., rate, uniformity, etc.). The main disadvantage of fluid models is that only "average" values of the dependent variables are obtained, instead of the corresponding distribution functions. There are situations where knowledge of distribution functions is absolutely necessary, for example, the ion energy and angular distributions on the wafer are critical to micro-feature profile evolution. Kinetic models provide the distribution functions as an output of the simulation. Also, kinetic models are considered more accurate than fluid models, especially at low pressures when the Knudsen number,  $Kn = \lambda/L > 0.1$ . Kinetic simulations, however, are computationally expensive when compared to fluid simulations.

Hybrid models are derived by combinations of primary models and have been developed in an attempt to preserve the accuracy and wealth of information of kinetic models, as well as the computational efficiency of fluid models. A brief tutorial of hybrid modeling of LTP and representative simulation results using hybrid models were presented in this work. Whenever possible, hybrid simulations were compared to kinetic and/or fluid simulations as well as experimental data.

There are many situations where hybrid models provide the accuracy of kinetic models with much reduced computational load. In practice, the reliability of the simulation in making quantitative predictions may be limited by the uncertainty in the transport and reaction parameters used in the simulation.<sup>[74]</sup> This is particularly acute in the case of industrial processes where complex mixed gas plasmas are used for etching and deposition. Description of the chemistry in these systems (especially surface chemistry which dominates at low pressures) is a formidable task.<sup>[75]</sup>

Ultimately, the kind of model to be used depends on the goal. For example, if the goal is to understand new physics, a kinetic model may be most suitable. If the goal is to do parametric investigations for plasma reactor design, a judiciously selected fluid or hybrid model may be most appropriate. In any case, one thing is certain: modeling and simulation of plasmas will continue to be an indispensable tool of LTP science and engineering.

Acknowledgements: This work was supported by the National Science Foundation grant PHY-1500518, and the Department of Energy, Office of Fusion Energy Science, contract DE-SC0001939.

Received: July 21, 2016; Revised: August 17, 2016; Accepted: August 23, 2016; DOI: 10.1002/ppap.201600152

Keywords: hybrid simulations; low temperature plasmas; modeling; multiscale simulations; radio frequency glow discharges

- [1] H. C. Kim, F. Iza, S. S. Yang, M. Radmilovic-Radjenov, J. K. Lee, *J. Phys. D: Appl. Phys.* **2005**, *38*, R283.
- [2] D. J. Economou, *Thin Solid Films* **2000**, *365*, 348.
- [3] G. G. Lister, *J. Phys. D: Appl. Phys.* **1992**, *25*, 1649.
- [4] D. Lymberopoulos, D. J. Economou, *IEEE Trans. Plasma Sci.* **1995**, *23*, 573.
- [5] S. Markidis, P. Henri, G. Lapenta, K. Ronnmark, M. Hamrin, Z. Meliani, E. Laure, *J. Comp. Phys.* **2014**, *271*, 415.
- [6] T. Amano, K. Higashimori, K. Shirakawa, *J. Comp. Phys.* **2014**, *275*, 197.
- [7] H. C. Kim, J. K. Lee, *J. Vac. Sci. Technol. A* **2005**, *23*, 651.
- [8] D. J. Economou, *J. Vac. Sci. Technol. A* **2013**, *31*, 050823.
- [9] V. A. Godyak, R. B. Piejak, B. M. Alexandrovich, *Phys. Rev. Lett.* **1992**, *68*, 40.
- [10] V. A. Godyak, R. B. Piejak, *Phys. Rev. Lett.* **1990**, *65*, 996.
- [11] M. A. Lieberman, A. J. Lichtenberg, "Principles of Plasma Discharges and Materials Processing", 2nd edition, Wiley, New York **2005**.
- [12] M. A. Lieberman, R. A. Gottscho, "Design of High Density Plasma Sources for Materials Processing", in *Physics of Thin Films*, M. Francombe, J. Vossen, Eds., Academic Press, San Diego, CA **1993**.
- [13] J. Hopwood, *Plasma Sources Sci. Technol.* **1992**, *1*, 109.
- [14] J. H. Keller, J. C. Foster, M. S. Barnes, *J. Vac. Sci. Technol. A* **1993**, *11*, 2487.
- [15] E. Gogolides, H. H. Sawin, *J. Appl. Phys.* **1992**, *72*, 3971.
- [16] D. P. Passchier, W. J. Goedheer, *J. Appl. Phys.* **1993**, *74*, 3744.
- [17] D. B. Graves, K. F. Jensen, *IEEE Trans. Plasma Sci.* **1986**, *14*, 78.
- [18] S.-K. Park, D. J. Economou, *J. Appl. Phys.* **1990**, *68*, 3904.
- [19] M. Meyyappan, Ed., "Computational Modeling in Semiconductor Processing", Artech House, Boston, MA **1994**.
- [20] A. D. Richards, B. E. Thompson, H. H. Sawin, *Appl. Phys. Lett.* **1987**, *50*, 492.
- [21] V. A. Godyak, "Soviet Radio Frequency Discharge Research", Delphic Associates Inc, Falls Church, VA **1986**.
- [22] C. G. Goedde, A. J. Lichtenberg, M. A. Lieberman, *J. Appl. Phys.* **1988**, *64*, 4375.
- [23] M. Surendra, D. Vender, *Appl. Phys. Lett.* **1994**, *65*, 153.
- [24] M. M. Turner, *Plasma Sources Sci. Technol.* **1996**, *5*, 159.
- [25] Y. Oh, N. Choi, D. Choi, *J. Appl. Phys.* **1990**, *67*, 3264.
- [26] D. P. Lymberopoulos, D. J. Economou, *Appl. Phys. Lett.* **1993**, *63*, 2478.
- [27] Q. Wang, D. J. Economou, V. M. Donnelly, *J. Appl. Phys.* **2006**, *100*, 023301.
- [28] J. D. Bukowski, D. B. Graves, *J. Appl. Phys.* **1996**, *80*, 2614.
- [29] M. Meyyappan, T. R. Govindan, *J. Vac. Sci. Technol. A* **1992**, *10*, 1344.
- [30] M. H. Wilcoxson, V. I. Manousiouthakis, *J. Comp. Phys.* **1994**, *115*, 376.
- [31] D. Breden, L. L. Raja, *Plasma Sources Sci. Technol.* **2014**, *23*, 065020.
- [32] D. P. Lymberopoulos, D. J. Economou, *J. Vac. Sci. Technol. A* **1994**, *12*, 1229.
- [33] D. P. Lymberopoulos, D. J. Economou, *J. Res. Natl. Inst. Stand. Technol.* **1995**, *100*, 473.
- [34] J. D. Bukowski, D. B. Graves, *J. Appl. Phys.* **1996**, *80*, 2614.
- [35] P. J. Chantry, *J. Appl. Phys.* **1987**, *62*, 1141.
- [36] C. K. Birdsall, A. B. Langdon, "Plasma Physics via Computer Simulation", McGraw-Hill, New York **1985**.
- [37] C. K. Birdsall, *IEEE Trans. Plasma Sci.* **1991**, *19*, 65.
- [38] V. Vahedi, G. DiPeso, C. K. Birdsall, M. A. Lieberman, T. D. Ronglien, *Plasma Sources Sci. Technol.* **1993**, *2*, 261.
- [39] M. Surendra, M. Dalvie, *Phys. Rev. E* **1993**, *48*, 3914.
- [40] G. A. Bird, "Molecular Gas Dynamics and the Direct Simulation of Gas Flows". Oxford Science Publications, Oxford **1994**.
- [41] E. S. Oram, C. K. Oh, B. Z. Cybyk, *Annu. Rev. Fluid Mech.* **1998**, *30*, 403.
- [42] D. J. Economou, T. Bartel, R. Wise, D. Lymberopoulos, *IEEE Trans. Plasma Sci.* **1995**, *23*, 581.
- [43] J. Johannes, T. Bartel, G. A. Hebner, J. Woodworth, D. J. Economou, *J. Electrochem. Soc.* **1997**, *144*, 2448.
- [44] M. E. Riley, K. E. Greenberg, G. A. Hebner, P. Drallos, *J. Appl. Phys.* **1994**, *75*, 2789.
- [45] D. Loffhagen, F. Sigenege, *Plasma Sources Sci. Technol.* **2009**, *18*, 034006.
- [46] V. Vahedi, M. Surendra, *Comput. Phys. Commun.* **1995**, *87*, 179.
- [47] U. Kortshagen, I. Pukropski, L. D. Tsendin, *Phys. Rev. E* **1995**, *51*, 6063.
- [48] N. Sato, H. Tagashira, *IEEE Trans. Plasma Sci.* **1991**, *19*, 102.
- [49] P. L. G. Ventzek, R. J. Hoekstra, M. J. Kushner, *J. Vac. Sci. Technol. B* **1994**, *12*, 461.
- [50] A. Bogaerts, R. Gijbels, W. J. Goedheer, *J. Appl. Phys.* **1995**, *78*, 2233.
- [51] I. B. Bernstein, T. Holstein, *Phys. Rev.* **1954**, *94*, 1475.
- [52] L. D. Tsendin, *Sov. Phys. JETP* **1974**, *39*, 805.
- [53] V. I. Kolobov, V. A. Godyak, *IEEE Trans. Plasma Sci.* **1995**, *23*, 503.
- [54] U. Kortshagen, B. G. Heil, *IEEE Trans. Plasma Sci.* **1999**, *27*, 1297.
- [55] J. Matsui, M. Shibata, N. Nakano, T. Makabe, *J. Vac. Sci. Technol. A* **1998**, *16*, 294.
- [56] M. J. Kushner, *J. Phys. D: Appl. Phys.* **2009**, *42*, 194013.
- [57] A. Bogaerts, *Plasma Sources Sci. Technol.* **1999**, *8*, 210.
- [58] G. J. M. Hagelaar, L. C. Pitchford, *Plasma Sources Sci. Technol.* **2005**, *14*, 722.
- [59] S. W. Hwang, H.-J. Lee, H. J. Lee, *Plasma Sources Sci. Technol.* **2014**, *23*, 065040.
- [60] M. M. Turner, *Plasma Sources Sci. Technol.* **2016**, *25*, 015003.
- [61] R. S. Wise, D. P. Lymberopoulos, D. J. Economou, *Plasma Sources Sci. Technol.* **1995**, *4*, 317.
- [62] N. A. Gatsonis, X. Yin, *J. Propul. Power* **2001**, *17*, 945.

- [63] M. Shimada, G. R. Tynan, R. Cattolica, *J. Appl. Phys.* **2008**, *103*, 033304.
- [64] S. K. Nam, D. J. Economou, V. M. Donnelly, *Plasma Sources Sci. Technol.* **2007**, *16*, 90.
- [65] S. K. Nam, D. J. Economou, V. M. Donnelly, *IEEE Trans. Plasma Sci.* **2007**, *35*, 1370.
- [66] D. T. K. Kwok, *J. Comp. Phys.* **2008**, *227*, 5758.
- [67] P. Diomede, S. Longo, D. J. Economou, M. Capitelli, *J. Phys. D: Appl. Phys.* **2012**, *45*, 175204.
- [68] E. Kawamura, V. Vahedi, M. A. Lieberman, C. K. Birdsall, *Plasma Sources Sci. Technol.* **1999**, *8*, R45.
- [69] D. O'Connell, R. Zorat, A. R. Ellingboe, M. M. Turner, *Phys. Plasmas* **2007**, *14*, 103510.
- [70] D. Eremin, T. Hemke, T. Mussenbrock, *Plasma Sources Sci. Technol.* **2016**, *25*, 150009.
- [71] M. Surendra, *Plasma Sources Sci. Technol.* **1995**, *4*, 56.
- [72] B. Ramamurthi, D. J. Economou, I. Kaganovich, *Plasma Sources Sci. Technol.* **2003**, *12*, 170.
- [73] V. A. Godyak, R. P. Piejak, *J. Appl. Phys.* **1997**, *82*, 5944.
- [74] M. M. Turner, *Plasma Sources Sci. Technol.* **2015**, *24*, 035027.
- [75] S.-X. Zhao, Y.-R. Zhang, F. Gao, Y.-N. Wang, A. Bogaerts, *J. Appl. Phys.* **2015**, *117*, 243303.